Journal of Polymer Research (2020) 27:173
https://doi.org/10.1007/s10965-020-02154-w

ORIGINAL PAPER

Competing hydrogen bonding produces mesoporous/macroporous carbons templated by a high-molecular-weight poly(caprolactone–*b*–ethylene oxide–*b*–caprolactone) triblock copolymer

Wei-Shih Hung[1] · Mahmoud MM Ahmed[1] · Mohamed Gamal Mohamed[1] · Shiao-Wei Kuo[1,2]

Received: 24 February 2020 / Accepted: 6 May 2020
© The Polymer Society, Taipei 2020

Abstract

In this study we developed a simple strategy to synthesize macro- and mesoporous carbons by using a high-molecular-weight triblock copolymer, PCL_{440}-*b*-PEO_{454}-*b*-PCL_{440} (CEC), as a single template, itself prepared through simple ring-opening polymerization from a commercial homopolymer (HO-PEO_{454}-OH) as the bifunctional macroinitiator and a resol-type phenolic resin as the carbon source. We employed differential scanning calorimetry, Fourier transform infrared (FTIR) spectroscopy, and small-angle X-ray scattering to investigate the thermal behavior, hydrogen bonding, and self-assembled nanostructures of the phenolic/CEC blends. We obtained macro- and mesoporous carbons possessing cylinder or spherical micelle structures with large pores (> 50 nm) and high surface areas (>400 m^2 g^{-1}), the result of most of the phenolic OH units preferring to interact (based on FTIR spectral analyses) with the PEO segment rather than the PCL segment. These macro/mesoporous carbons displayed reasonable CO_2 uptake and energy storage behavior.

Keywords Mesoporous carbon · Self-assembly · Hydrogen bonding · Triblock copolymer · Supercapacitors

Introduction

Porous materials featuring high surface areas and large pore volumes have many possible applications in, for example, separation, catalysis, drug delivery, adsorption, and energy storage.[1–6] The IUPAC has classified three kinds of porous materials, depending on their pore sizes[7]: microporous materials (<2 nm), mesoporous materials (2–50 nm), and macroporous materials (>50 nm).

Although mesoporous materials are generally synthesized through the use of phase separation, foaming, molecular imprinting, and hard-template methods, such approaches yield well-defined ordered mesoporous materials.[7–10] Block copolymers often self-assemble into structures having various forms after blending with other block copolymers, homopolymers, or block copolymer mixtures capable of competing for hydrogen bonding interactions.[11–20] Indeed, through this approach, block copolymer/homopolymer blends have been used to obtain many types of mesoporous materials, including silicas, phenolic resins, and carbons.[21–25] Although the commercial Pluronic-type triblock copolymer poly(ethylene oxide–*b*–propylene oxide–*b*–ethylene oxide) has been used widely as a template for the preparation of mesoporous materials, limitations in the molecular weights of Pluronic-type triblock copolymers have made it difficult to synthesize mesoporous carbons this way with pore sizes greater than 10 nm.[26–31] PEO-based diblock copolymers featuring long hydrophobic segments of high molecular weight—for example, poly(ethylene oxide–*b*–methyl methacrylate) (PEO-*b*-PMMA), poly(ethylene oxide–*b*–styrene) (PEO-*b*-PS), and poly(ethylene oxide–*b*–caprolactone) (PEO-*b*-PCL)—are

Electronic supplementary material The online version of this article (https://doi.org/10.1007/s10965-020-02154-w) contains supplementary material, which is available to authorized users.

✉ Shiao-Wei Kuo
kuosw@faculty.nsysu.edu.tw

[1] Department of Materials and Optoelectronic Science, Center of Crystal Research, National Sun Yat-Sen University, Kaohsiung 80424, Taiwan

[2] Department of Medicinal and Applied Chemistry, Kaohsiung Medical University, Kaohsiung 807, Taiwan

Published online: 21 May 2020

promising candidate templates for the synthesize of large mesoporous carbons.[32–40] Indeed, PEO_{114}-*b*-$PMMA_{114}$, PEO_{114}-*b*-PS_{102}, PEO_{114}-*b*-PS_{230}, and PEO_{114}-*b*-PCL_{87} diblock copolymers have been used as templates to prepare long-range-ordered mesoporous carbons; for example, the largest pore size of approximately 23 nm was obtained when templating with the largest molecular weight of the PEO-*b*-PS diblock copolymer (PEO_{125}-*b*-PS_{230}).[32–40] Furthermore, Wiesner et al. used a high-molecular-weight (ca. 100,000 g mol^{-1}) PEO-*b*-PS-*b*-PI triblock copolymer as the template to obtain a mesoporous carbon having an average pore size of approximately 39 nm—the largest pores formed when using a single block copolymer as the template.[41]

To further increase their pore sizes, Zhao et al. used PEO-*b*-PS/PS and PEO-*b*-PMMA/PMMA blends as templates to prepare ultralarge mesoporous carbons; here, the PS and PMMA homopolymers acted as pore expanders.[42,43] Nevertheless, disordered porous structures having multimodal pore size distributions (ca. 40–90 nm) were obtained when the homopolymer concentrations were greater than 20 wt%, because of macrophase separation occurred under such conditions.[42, 43] Because both the PEO-*b*-PMMA or PEO-*b*-PS diblock copolymers were synthesized through atom transfer radical polymerization, using chain-end-modified PEO segments (e.g., PEO-Br) as macroinitiators, it was difficult to prepare them with high molecular weights.[32–35]

In this study, we synthesized a high-molecular-weight (ca. 120,000 g mol^{-1}) triblock copolymer, PCL_{440}-*b*-PEO_{454}-*b*-PCL_{440} (CEC), through simple ring-opening polymerization (ROP) from commercial HO-PEO_{454}-OH as the macroinitiator. After applying thermal curing, calcination, and carbonization procedures (Scheme 1), we obtained a few mesoporous (30–50 nm) and large amounts of macroporous (>50 nm) carbons when using the CEC triblock copolymer as a single template along with a resol-type phenolic resin as the carbon source. We investigated the thermal behavior, hydrogen bonding, and self-assembled structures of various phenolic/CEC blends, and then examined the pore sizes, structures, surface areas, and pore volumes of the resulting macro/mesoporous carbons. Herein, we also discuss the CO_2 capture and energy storage behavior of these easy-to-prepare large macro/mesoporous carbons (>50 nm).

Experimental section

Materials

The triblock copolymer PCL_{440}-*b*-PEO_{454}-*b*-PCL_{440} (CEC) was synthesized through ROP from caprolactone, dihydroxyl-terminated poly(ethylene oxide) (PEO_{454}), and stannous(II) octoate. A mixture of ε-caprolactone and

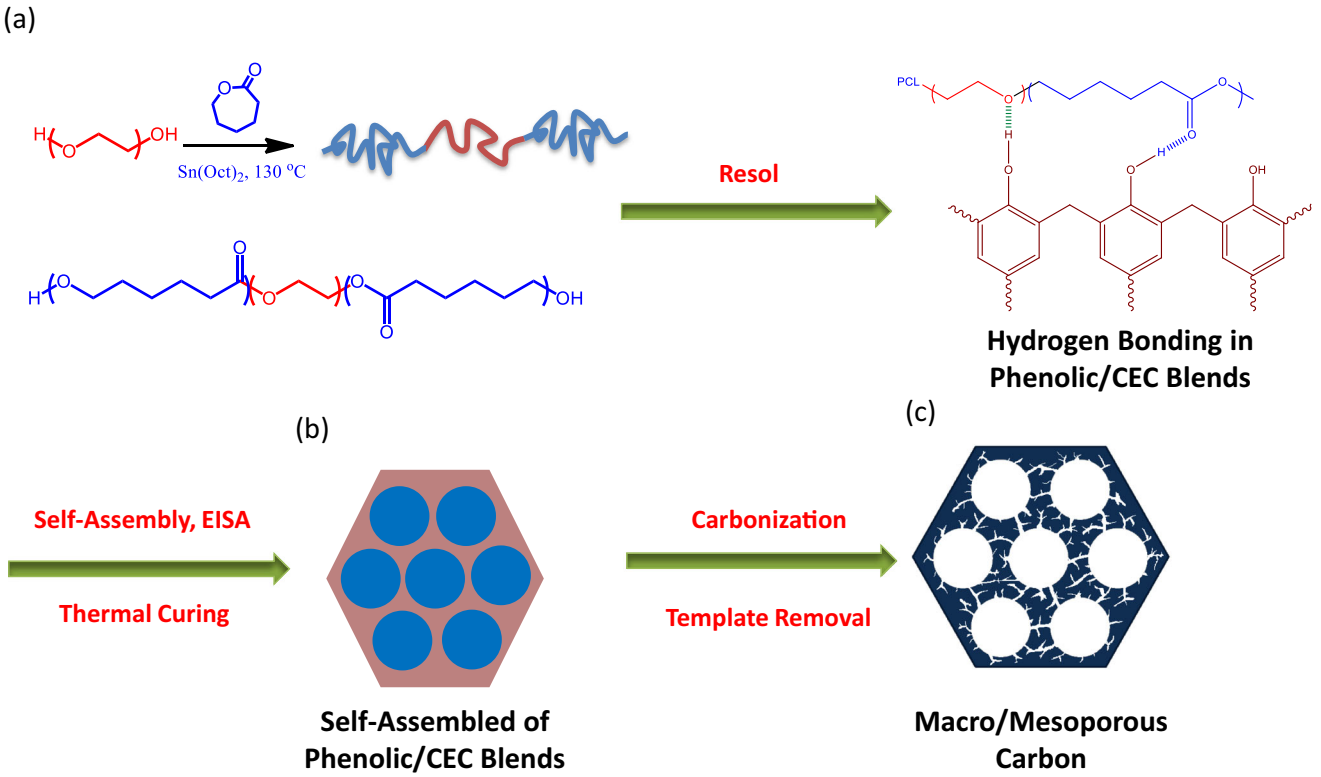

Scheme 1 Fabrication of (c) macro/mesoporous carbons templated by (a) a high-molecular-weight CEC triblock copolymer and (b) the self-assembled structures formed from phenolic/CEC blends through reaction-induced micro-phase separation.

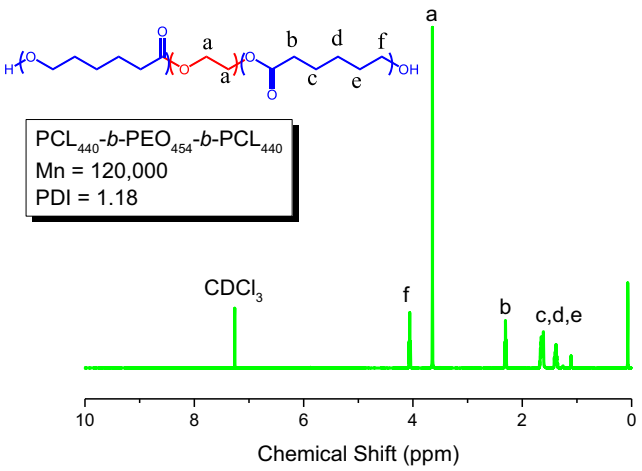

Fig. 1 ^{1}H NMR spectrum of CEC triblock copolymer prepared in this study

PEO_{454} under N_2 was treated with the catalyst (a small amount) and then stirred continuously at 130 °C for 24 h under a N_2 atmosphere. The PCL_{440}-*b*-PEO_{454}-*b*-PCL_{440} triblock copolymer was dissolved in CH_2Cl_2, precipitated in *n*-hexane and dried under vacuum at 40 °C. Phenolic resin (resol-type) having a molecular weight approximately 500 g mol^{-1} was prepared from phenol and formaldehyde through condensation in the presence of NaOH.[38, 39]

Macro/mesoporous carbons

Various compositions of phenolic/CEC blends dissolved in THF were stirred at room temperature for 2 days. The blend systems were poured into Teflon dishes and then the solvent was evaporated slowly at room temperature for 24 h [evaporation-induced self-assembly (EISA)]. For thermal curing of the phenolic resins, the dishes were heated in an oven at 150 °C for 2 days and then subjected to thermal calcination (heating up to 700 °C at 1 °C min^{-1}) to remove the templates and provide the macro/mesoporous carbons (Scheme 1).

Results and discussions

Characterization of phenolic/PCL-b-PEO-b-PCL blends

We prepared the PCL_{440}-*b*-PEO_{454}-*b*-PCL_{440} triblock copolymer, for use as the template, through ROP; ^{1}H NMR spectroscopy revealed its molecular weight (Fig. 1). The signal for the CH_2 units of the PEO block segment appeared at 3.65 ppm, while that for the OCH_2 units (peak f) of the PCL block segment appeared at 4.05 ppm. We determined the molecular weight from the ratio of these two peak areas, and obtained, through GPC analysis, a polydispersity (PDI) of 1.18 for this triblock copolymer. We synthesized mesoporous carbons from phenolic/CEC blends: their mesophases gradually formed during EISA, and then we applied thermal curing and carbonization processes to remove the template (Scheme 1).

In previous studies, we have investigated the hydrogen bonding interactions of phenolic with PEO and PCL segments. The inter-association equilibrium constant for the phenolic/PCL binary pair ($K_A = 116$) is smaller than that for phenolic/PEO ($K_A = 264$), indicating that the OH units of phenolic prefer to interact with PEO segments over PCL segments. Figure 2(a) presents the FTIR spectra (C=O absorption

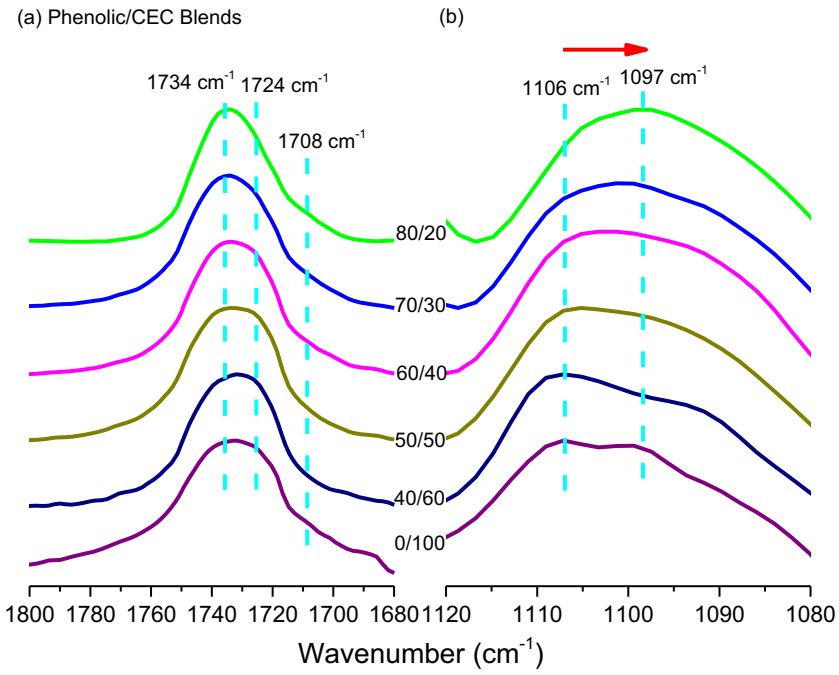

Fig. 2 FTIR spectra, measured at room temperature, of various phenolic/CEC blends: (a) C=O and (b) ether absorption regions

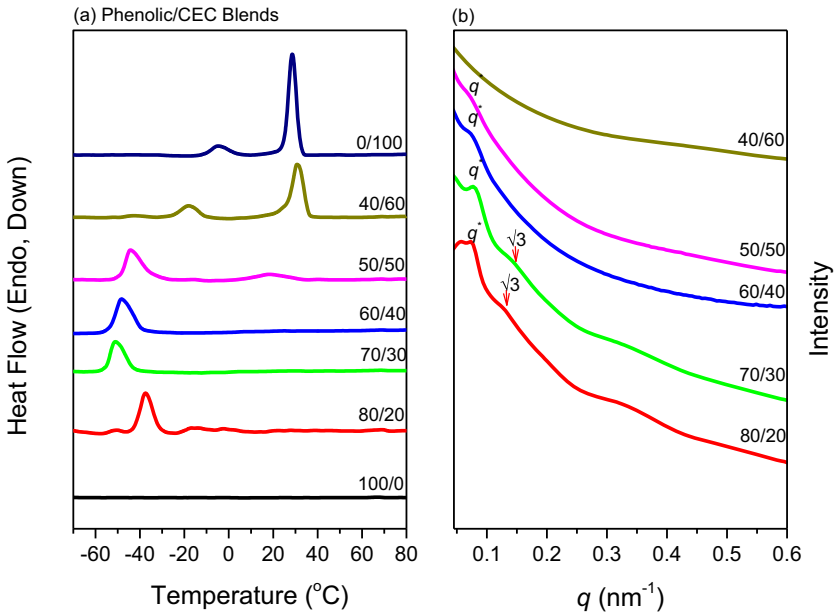

Fig. 3 (a) DSC cooling scans and (b) SAXS patterns of various phenolic/CEC blends

region) of various phenolic/CEC blends, recorded at room temperature. The spectrum of the pure CEC features two major signals at 1734 and 1724 cm^{-1}, representing the amorphous (or free) and crystalline phases, respectively, of the PCL segment.[44, 45] Upon increasing the concentration of phenolic, the fraction of the crystalline peak at 1724 cm^{-1} decreased and a shoulder signal appeared at 1708 cm^{-1}, representing hydrogen-bonded C=O units. Nevertheless, the area fraction of the hydrogen-bonded C=O groups in the phenolic/CEC = 80/20 blend was only 0.14, significantly lower than that (0.88) in the phenolic/PCL = 80/20 blend, as determined through curve fitting.[44, 45] Fig. 2(b) presents the ether absorption region of the FTIR spectra of the phenolic/CEC blends. The spectrum of the pure CEC featured a characteristic signal at 1106 cm^{-1}, due to the ether (C–O–C) units in the PEO segment. At a high phenolic concentration, this band shifted to 1097 cm^{-1}, representing the hydrogen-bonded C–O–C units. This behavior suggested that the phenolic OH units preferred to interact with the PEO segment, rather than the PCL segment, in the phenolic/CEC blends.[36–40]

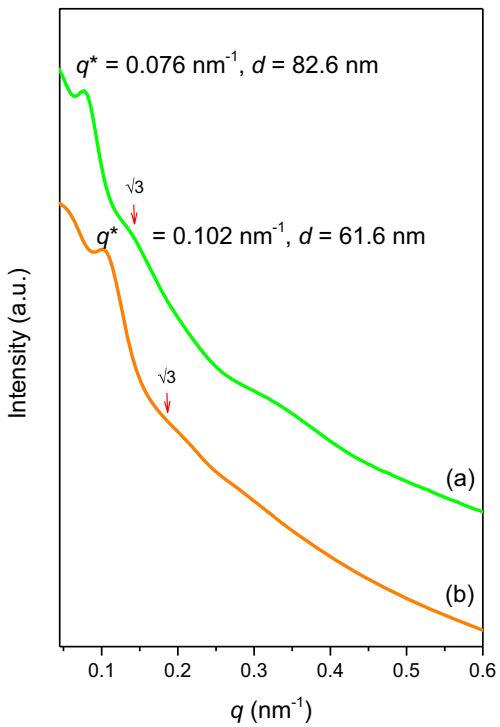

Fig. 4 SAXS patterns of (b) the macro/mesoporous carbon derived from (a) the phenolic/CEC = 70/30 blend

We used the cooling scans (cooling rate: 5 °C min^{-1}) of DSC thermograms to investigate the hydrogen bonding and self-assembly of our phenolic/CEC blends [Fig. 3(a)]. The freezing temperature (T_f) of the crystallization exotherm can be correlated to the self-assembled nanostructure formed through nonisothermal crystallization at a fixed cooling rate. The pure CEC provided values of T_f of 29 °C for the PEO segment and − 5 °C for the PCL segment, suggesting two microphase domains formed for this triblock copolymer. For the phenolic/CEC = 40/60 and 50/50 blends, we observed two exotherms at +30/−18 °C and + 18/−44 °C, respectively; the higher value presumably also represented crystallization of the PEO segment, while the lower value was not observed for either the PEO or PCL segment. In previous studies, we found that the degree of supercooling ($\Delta T = T_m^\circ - T_f$) is strongly dependent on the self-assembled nanostructures containing PCL segments ($T_m^\circ = 75$ °C) in confined crystallization; for example, we have measured degrees of supercooling for lamellar, cylinder, and spherical nanostructures to be approximately 75, 125, and 130 °C, respectively.[46] In this case,

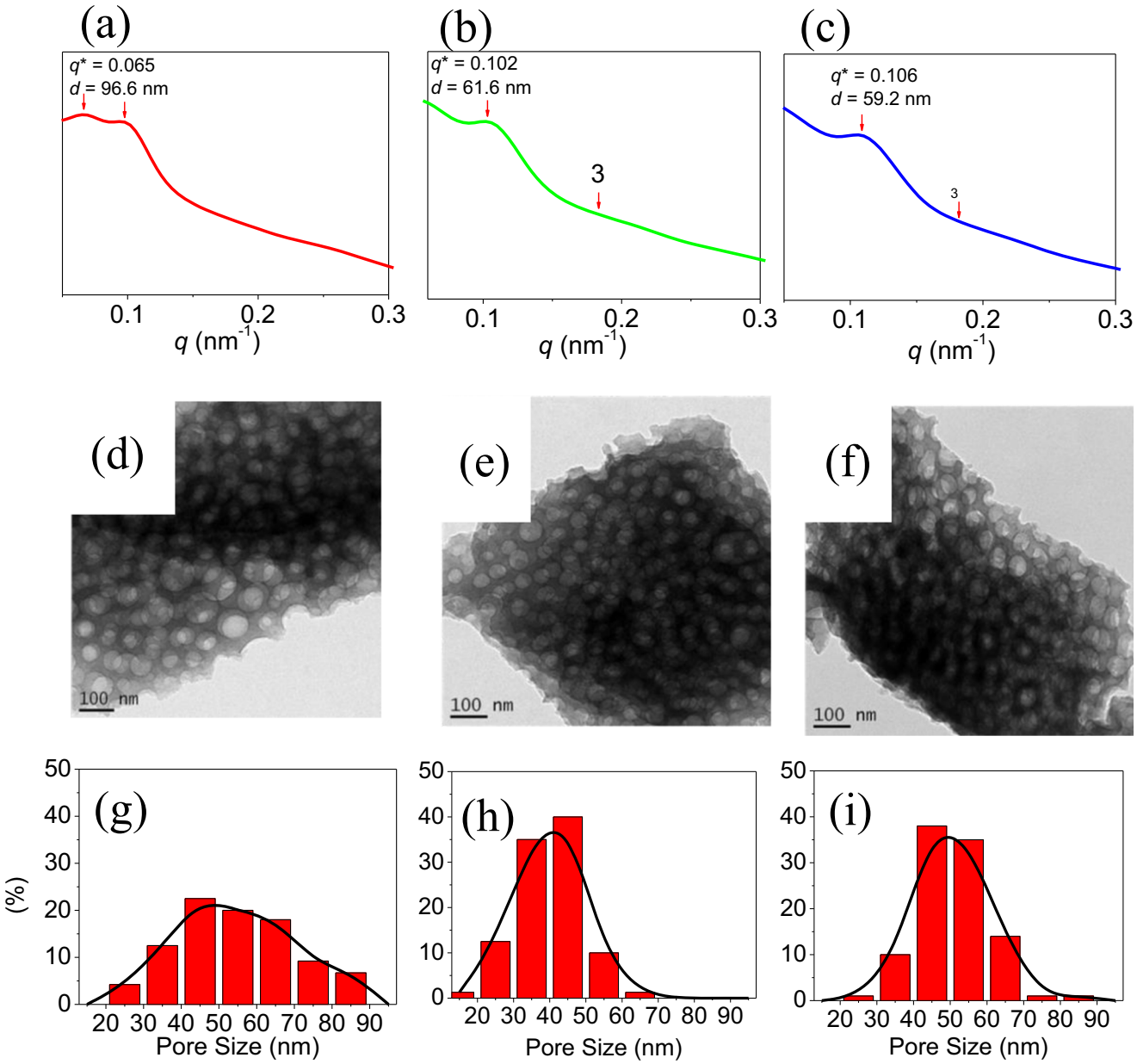

Fig. 5 (a–c) SAXS, (d–f) TEM, and (g–i) pore size distributions (based on TEM analyses) of the macro/mesoporous carbons derived from the phenolic/CEC (a, d, g) 80/20, (b, e, h) 70/30, and (c, f, i) 60/40 blends

because we observed the two exotherms, homogeneous crystallization of the PCL segment must not have occurred. The SAXS patterns of these phenolic/PCL-*b*-PEO-*b*-PCL = 40/60 and 50/50 blends exhibited [Fig. 3(b)] only disorder (40/60) and one broad peak (50/50), indicative of a disordered and a short-range-ordered or wormlike structure, respectively. Increasing the phenolic/CEC ratio to 60/40 and 70/30 resulted in only a single value of T_f for the PCL segment in each case, at −48 °C (ΔT = 123 °C) and − 50 °C (ΔT = 125 °C), respectively, presumably with a cylinder structure, as determined from the SAXS patterns featuring peak ratios of 1:√3 [Fig. 3(b)]. Further increasing the phenolic/CEC ratio to 80/20 led to the major value of T_f for the PCL segment appearing at −38 °C, also suggesting a cylinder or spherical micelle structure, as confirmed by the SAXS pattern having a peak ratio of 1:√3 [Fig. 3(b)].

Macro/Mesoporous carbons from phenolic/CEC blends

We thermally cured the phenolic matrix at 150 °C for 24 h and then used thermal calcination at 700 °C to remove the CEC template, thereby obtaining the macro/mesoporous carbons. Figures 4 presents SAXS analyses of the phenolic/CEC = 70/30 blend and its corresponding

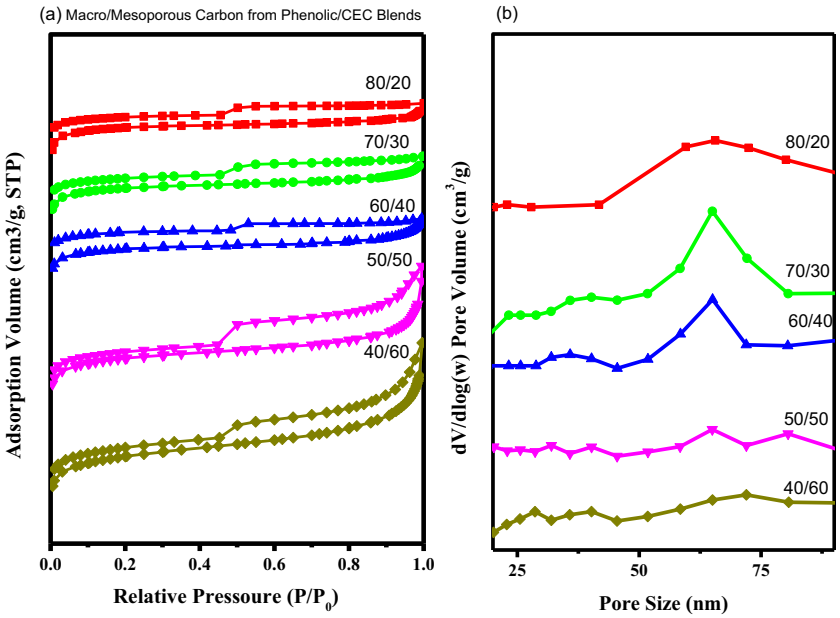

Fig. 6 (a) N_2 adsorption/desorption hysteresis isotherms and (b) pore size distributions of the macro/mesoporous carbons derived from various phenolic/CEC blends

porous carbon, measured at room temperature. The peak ratio did not change from 1:√3, but became sharper because the electron density contrast increased after pore formation (i.e., upon removal of the CEC template), suggesting that the original cylinder structure was maintained. In addition, the first scattering peak of the phenolic/CEC = 70/30 blend having a value of q^* of 0.076 nm^{-1} (d = 82.6 nm) shifted to a value of 0.102 nm^{-1} (d = 61.6 nm) after thermal calcination. Thus, the d-spacing decreased after thermal pyrolysis, due to the continuous removal of oxygen and hydrogen atoms to form the small pores of the carbon material.

Figures 5 and S1 display the SAXS patterns, TEM images, and corresponding pore size distributions (based on the TEM images) of the porous carbons obtained from the corresponding phenolic/CEC blends. Figure 5(a) presents the SAXS pattern of the porous carbon derived from the phenolic/CEC = 80/20 blend; the two broad peaks indicated that at least two different pore sizes self-assembled from the cylinder or spherical micelle structure. This feature was confirmed from the TEM images in Fig. 5(d); the broad pore size distribution, based on TEM images, is provided in Fig. 5(g). The first peak corresponded to a value of q^* of 0.065 nm^{-1} (d = 96.6 nm); thus, the pore size distribution ranged from 20 to 90 nm. This material could, therefore, be classified as a macroporous and mesoporous carbon. Figures 5(b) and 5(c) display the SAXS patterns of the mesoporous carbons obtained from the phenolic/CEC = 70/30 and 60/40 blends. Both patterns featured peak ratios of 1:√3, suggesting cylinder or spherical micelle structures, which were confirmed from the TEM images in Figs. 5(e) and 5(f), respectively. These two porous carbons had relatively narrow pore size distributions, but some of their pores were larger than 50 nm; therefore, these two compositions were presumably also macroporous and mesoporous carbons [Figs. 5(h) and 5(i)]. Furthermore, decreasing the phenolic/CEC ratios to 50/50 and 40/60 led to porous carbons having broad peaks in their SAXS patterns [Figs. S1(a) and S1(b), respectively], indicative of disordered porous structures, as confirmed by their TEM images [Figs. S1(c) and S1(d), respectively].

Figure 6(a) displays the N_2 sorption isotherms recorded to investigate the porous structures of these porous carbons. All featured typical type-IV curves and H_1-like hysteresis loops. Sharp capillary condensation steps occurred in the relative pressure (P/P_0) range from 0.8 to 1.0, suggesting that the porous structures possessed large and cylindrical pores, consistent with the SAXS patterns and TEM images. Figure 6(b) reveals that the average pore size distributions, determined

Table 1 Properties of macro/mesoporous carbons templated by CEC triblock copolymer in this study

Phenolic/CEC	d spacing $(nm)^{SAXS}$	Pore Size $(nm)^{BET}$	Pore Size $(nm)^{TEM}$	S_{BET} (m^2/g)	V_{Total} (cm^3/g)	V_{Meso} (cm^3/g)
80/20	96.6	68.4 ± 7.8	55.4 ± 7.2	393.1	0.23	0.07
70/30	61.6	57.2 ± 14.4	39.9 ± 4.0	384.0	0.23	0.07
60/40	59.2	57.2 ± 14.4	51.2 ± 4.8	336.5	0.21	0.07

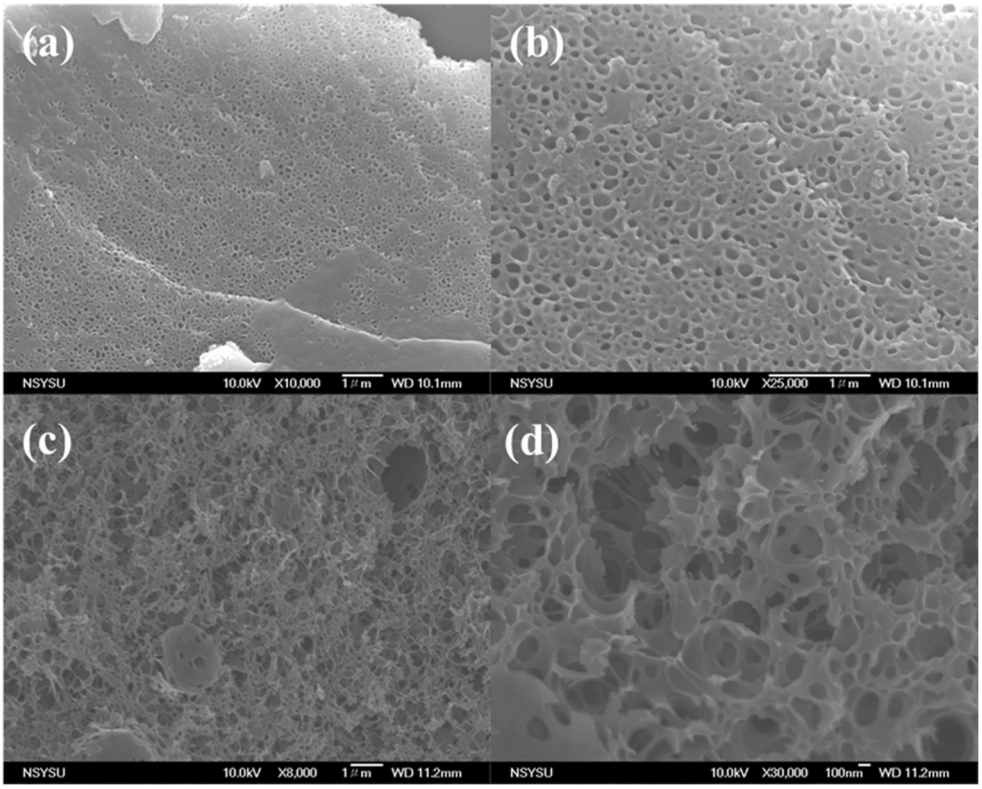

Fig. 7 FE-SEM images of the macro/mesoporous carbon derived from the phenolic/CEC = 60/40 blend: (a, b) top and (c, d) cross-sectional views

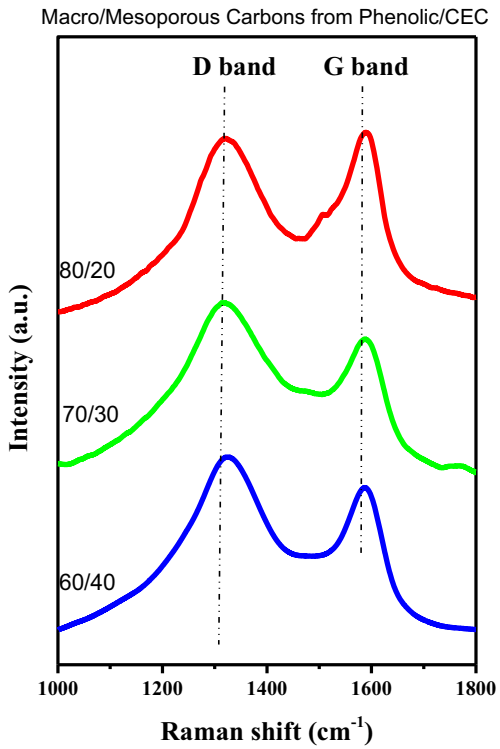

Fig. 8 Raman spectra of the macro/mesoporous carbons derived from the various phenolic/CEC blends

using the Harkins and Jura model, of the porous carbons derived from the phenolic/CEC = 80/20, 70/30, and 60/40 blends were 68.4, 57.2, and 57.2 nm, respectively. Table 1 summarizes the *d*-spacings, pore sizes, surface areas, and pore volumes of these macro/mesoporous carbons.

We also used FE-SEM to observe the pore structures in the macro/mesoporous carbon obtained from the phenolic/CEC = 60/40 blend. Figures 7(a) and 7(b) display top and side views; the short-range order of the macroporous structure is evident in Figs. 7(c) and 7(d). The mean pore size determined from the SEM images was 54.4 ± 10.6 nm (Fig. S2), close to those determined through BET analysis (57.2 ± 14.4 nm) and TEM imaging (51.2 ± 4.8 nm) of the same macro/mesoporous carbon. Thus, we conclude that both macro and mesoporous carbons were formed from the phenolic resin templated by our high-molecular-weight CEC triblock copolymer.

Raman spectroscopic, CO_2 capture, and electrochemical analyses of macro/mesoporous carbons

To further examine these macro/mesoporous carbons, we used Raman spectroscopy to investigate their intrinsic properties. The degree of graphitization can be determined roughly from the ratio of the intensities of the D- and G-bands (I_D/I_G), where the G-band is the signal of the sp^2-hybridized C–C bonds near 1587 cm^{-1}. Figure 8 presents the Raman spectra of our macro/

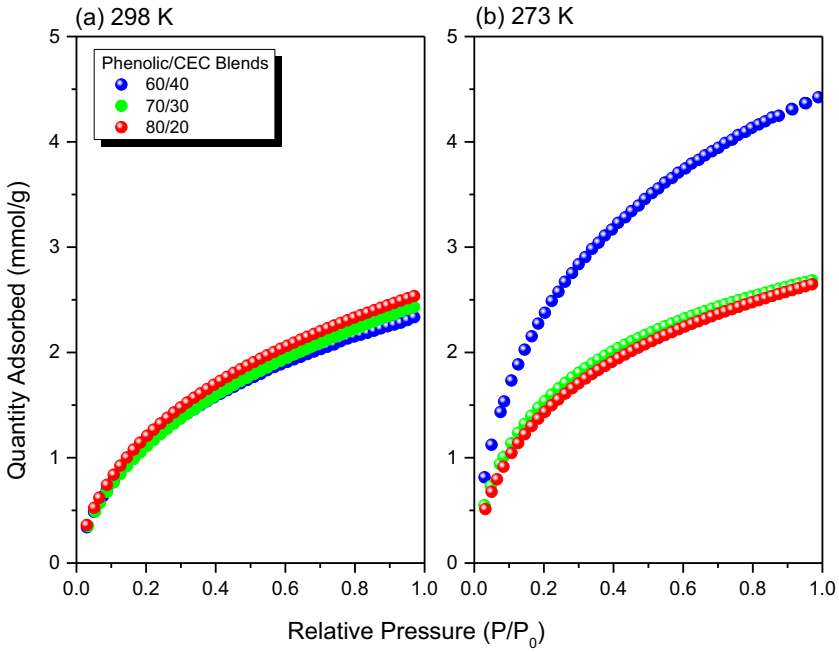

Fig. 9 CO_2 uptake properties of the macro/mesoporous carbons derived from the various phenolic/CEC blends, measured at (a) 298 and (b) 273 K

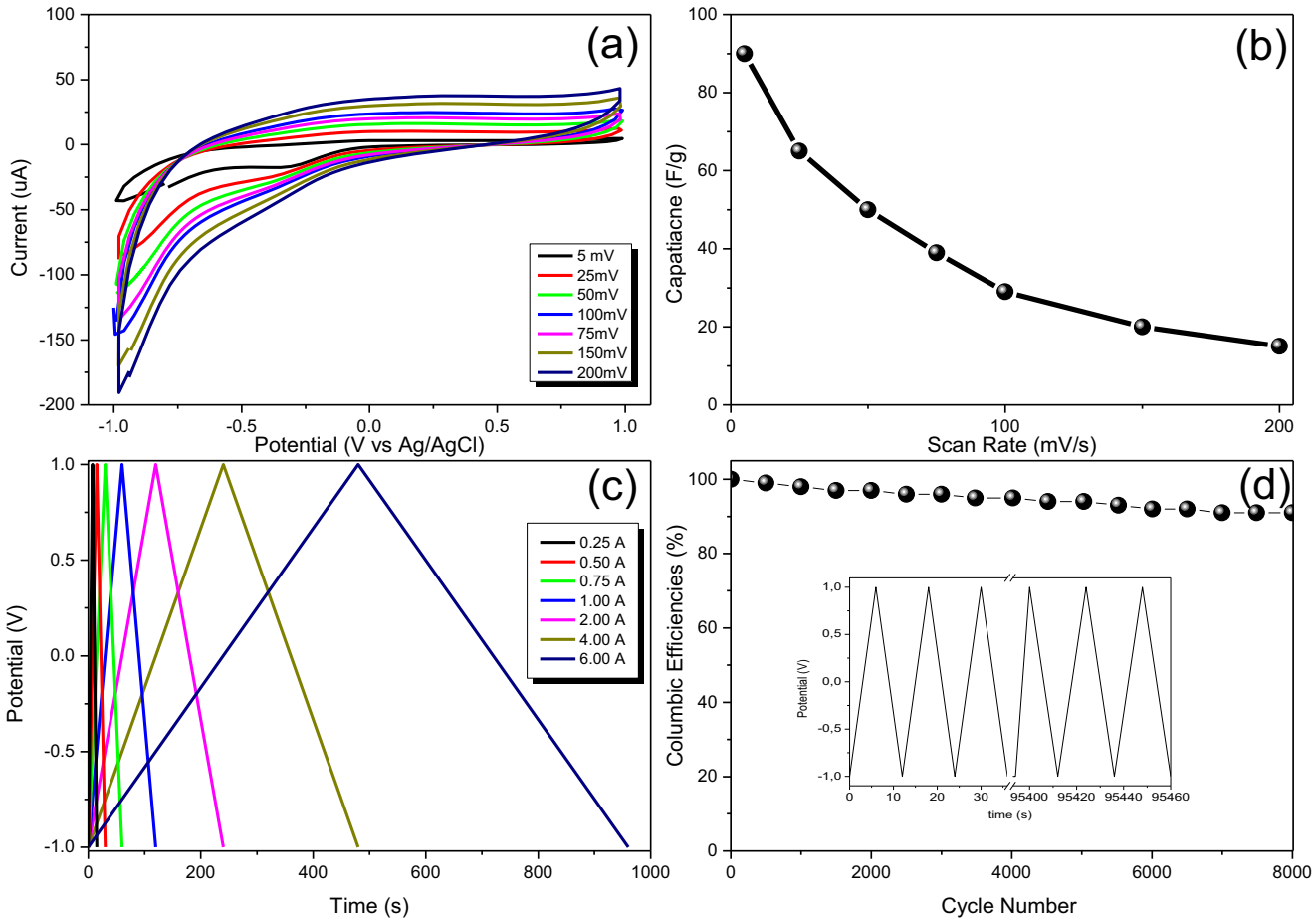

Fig. 10 (a) CV traces (scan rates: 5–200 mV s^{-1}), (b) capacitance plotted with respect to scan rate, (c) CDCs measured at various currents, and (d) Columbic efficiency measured at 20 A g^{-1} over 5000 cycles for the macro/mesoporous carbon derived from the phenolic/CEC = 60/40 blend

mesoporous carbons. The I_D/I_G ratios obtained from curve fitting of the spectra of the macro/mesoporous carbons derived from the phenolic/CEC = 80/20, 70/30, and 60/40 blends were 2.14, 2.34, and 2.51, respectively, suggesting that the structure of macro/mesoporous carbon from phenolic/CEC = 60/40 blend was much defected when compared with the other two macro/mesoporous carbons.

Their macro/mesoporous structures and high surface areas suggested that these macro/mesoporous carbons would be suitable for CO_2 capture. Figure 9 displays the CO_2 adsorption isotherms recorded at 298 and 273 K, respectively. The CO_2 capture capacities of the macro/mesoporous carbons obtained from the phenolic/CEC = 80/20, 70/30, and 60/40 blends were lower at 298 K (2.53, 2.43, and 2.33 mmol g^{-1}, respectively) than they were at 273 K (2.64, 2.68, and 4.42 mmol g^{-1}, respectively). More interestingly, the macro/mesoporous carbon derived from the phenolic/CEC = 60/40 blend exhibited [Fig. 9(b)] a much higher CO_2 uptake (4.42 mmol g^{-1}) at 273 K when compared with the other two macro/mesoporous carbons measured at the same temperature. We used the Clausius–Clapeyron equation[2] to calculate the heats of adsorption (Q_{st}) based on the CO_2 uptake data measured at 298 and 273 K. Again, the highest value of Q_{st} (37.12 kJ mol^{-1}) was that for the macro/mesoporous carbon obtained from the phenolic/CEC = 60/40 blend; the other two macro/mesoporous carbons derived from the phenolic/CEC = 70/30 and 80/20 blends gave values of 18.02 and 8.23 kJ mol^{-1}, respectively, at 1.0 mmol g^{-1}. We suspect that the more highly defected structure of the macro/mesoporous carbon obtained from the phenolic/CEC = 60/40 blend may have been responsible for the larger value of Q_{st} for its CO_2 uptake.[47–49]

It is essential that macro/mesoporous carbons developed for energy storage display high efficiencies. Herein, we selected the macro/mesoporous carbon derived from the phenolic/CEC = 60/40 blend for examination of its electrochemical performance in a three-electrode cell containing 1.0 M KCl as a green medium.[50] These conditions provides an extremely wide potential window for the CV curves (from −1.0 to +1.0 V) recorded for this macro/mesoporous carbon [Fig. 10(a)]. The CV curves revealed the behavior of a wide electric double layer capacitor (EDLC) with only the minor effect of a pseudocapacitor (PC); a much higher area of the EDLC was evident at all scan rates [Fig. 10(b)]. The capacitance value at 5 mV s^{-1} reached 90 F g^{-1} for this macro/mesoporous carbon. This high EDLC performance was presumably related to the major effect of the carbonization procedure in providing a high surface area for electron transfer on the electrode surface. We recorded the charge/discharge curves (CDC) at 2.0 A g^{-1} over the potential range from −1.0 to +1.0 V. The CDC curves were typically symmetrical, suggesting that the hybridization did not induce a resistive structure [Fig. 10(c)]. The electrodes displayed efficient stability at 2.0 A g^{-1} for 5000 cycles with 95% retention, as well as approximately 100% columbic efficiency [Fig. 10(d)]. Compared with other porous carbons, these results were characterized by exceptionally negligible IR drop curves having excellent symmetrical triangular shapes and a wide potential range. Furthermore, other porous carbons have not displayed such strong performance. In other words, these results suggest performance higher than that of other phenolic carbons used for energy storage (e.g., lignin-derived porous carbons have reached a specific capacitance of 100 F g^{-1} at 5 mV). Thus, our results are competitive with those of other reported structures having similar components.[51, 52] Wang et al. investigated the performance of an activated carton box having a surface area of greater than 2700 m^2 g^{-1} and obtained a capacitance that decreased significantly in terms of its retention and cycling abilities.[53] Besides, Zhao et al. are also much higher than other activated bamboo-like carbons composited with metal oxides (e.g., V_2O_5).[54] Table S1 summarizes the performance of other comparable materials. Indeed, our macro/mesoporous carbon derived from the phenolic/CEC = 60/40 blend appears to be a promising candidate material for energy storage applications.

Conclusion

We have synthesized ultralarge-pore mesoporous carbons when using the high-molecular-weight triblock copolymer CEC as a single template for resol acting as the carbon source. Competing hydrogen bonding interactions in the phenolic/PEO and phenolic/PCL phases induced the self-assembly of cylinder or spherical micelles from the CEC/resol blends. After carbonization, we obtained ultralarge-pore carbons having macroporous (>50 nm) structures and high surface areas (> 400 m^2 g^{-1}), suitable for use in CO_2 uptake and supercapacitor applications. The higher degree of defects (determined from Raman spectral analyses, with a higher value of I_D/I_G) in the structure of the macro/mesoporous carbon derived from the phenolic/CEC = 60/40 blend corresponded to a greater value of Q_{st} for its CO_2 uptake, and also to its highly efficient capacitance behavior (90 F g^{-1} at 5 mV s^{-1}) and excellent stability (95% after 5000 cycles). Thus, this simple approach allows the preparation of ultralarge-pore mesoporous carbons, templated by a high-molecular-weight triblock copolymer that mediated competing hydrogen bonding interactions, suitable for CO_2 uptake and electrochemical applications.

Acknowledgments This study was supported financially by the Ministry of Science and Technology, Taiwan, under contracts MOST 106-2221-E-110- 067-MY3, 108-2638-E-002-003-MY2, and 108-2221-E-110 -014-MY3.

References

1. Davis ME (2002) Ordered porous materials for emerging applications. Nature 417:813–821

2. AFM EL-M, Young C, Kim J, You J, Yamauchi Y, Kuo SW (2019) Hollow Microspherical and Microtubular [3+3] Carbazole-Based Covalent Organic Frameworks and Their Gas and Energy Storage Applications. ACS Appl Mater Interfaces 11:9343–9354
3. Wang C, Wang TM, Wang QH (2019) Ultralow-dielectric, nanoporous poly(methyl silsesquioxanes) films templated by a self-assembled block copolymer upon solvent annealing. J Polym Res 26:5
4. Wang ZB, Qiang HW, Zhang CL, Zhu ZH, Chen M, Chen CN, Zhang DW (2018) Facile fabrication of hollow polyaniline spheres and its application in supercapacitor. J Polym Res 25:129
5. El-Mahdy AFM, Mohamed MG, Mansoure TH, Yu HH, Chen T, Kuo SW (2019) Ultrastable tetraphenyl-p-phenylenediamine-based covalent organic frameworks as platforms for high-performance electrochemical supercapacitors. Chem Commun 55:14890–14893
6. Wu YC, Lu YS, Bastakoti BP, Li Y, Pramanik M, Hossain MS, Yanmaz E, Kuo SW (2016) Mesoporous TiO2 Thin Film Formed From a Bioinspired Supramolecular Assembly. ChemistrySelect 1: 4295–4299
7. Rouquerol J, Avnir D, Fairbridge CW, Everett DH, Haynes JM, Pernicone N, Ramsay JDF, Sing KSW, Unger KK (1994) Recommendations for the characterization of porous solids. Pure Appl Chem 66:1739–1758
8. Langley PJ, Hulliger J (1999) Nanoporous and mesoporous organic structures: new openings for materials research. Chem Soc Rev 28: 279–291
9. Dawson R, Cooper I, Adams DJ (2012) Nanoporous organic polymer networks. Prog Polym Sci 37:530–563
10. Muylaert I, Verberckmoes A, Decker JD, Voort PVD (2012) Ordered mesoporous phenolic resins: highly versatile and ultra stable support materials. Adv Colloid Interf Sci 175:39–51
11. Dobrosielska K, Wakao S, Takano A, Matsushita Y (2008) Nanophase-separated structures of AB block copolymer/C homopolymer blends with complementary hydrogen-bonding interactions. Macromolecules 41:7695–7698
12. Lee HF, Kuo SW, Huang CF, Lu JS, Chan SC, Wang CF, Chang FC (2006) Hydrogen-bonding interactions mediate the phase behavior of an AB/C block copolymer/homopolymer blend comprising poly (methyl methacrylate-b-vinylpyrrolidone) and poly (vinylphenol). Macromolecules 39:5458–5465
13. Kwak J, Han SH, Moon HC, Kim JK, Koo J, Lee JS, Pryamitsyn V, Ganesan V (2015) Phase behavior of binary blend consisting of asymmetric polystyrene-block-poly(2-vinylpyridine) copolymer and asymmetric deuterated polystyrene-block-poly(4-hydroxystyrene) copolymer. Macromolecules 48:1262–1266
14. Miyase H, Asai Y, Takano A, Matsushita Y (2017) Kaleidoscopic tiling patterns with large unit cells from ABC star-shaped Terpolymer/Diblock copolymer blends with hydrogen bonding interaction. Macromolecules 50:979–986
15. Tsou CT, Kuo SW (2019) Competing Hydrogen Bonding Interaction Creates Hierarchically Ordered Self-Assembled Structures of PMMA-b-P4VP/PVPh-b-PS Mixtures. Macromolecules 52:8374–8383
16. Mao BH, AFM EL-M, Kuo SW (2019) Bio-inspired multiple complementary hydrogen bonds enhance the miscibility of conjugated polymers blended with polystyrene derivatives. J Polym Res 26: 208
17. Kwak J, Han SH, Moon HC, Kim JK (2015) Effect of the degree of hydrogen bonding on asymmetric lamellar microdomains in binary block copolymer blends. Macromolecules 48:6347–6352
18. Tseng TC, Kuo SW (2019) Hydrogen bonding induces unusual self-assembled structures from mixtures of two miscible disordered diblock copolymers. Eur Polym J 116:361–369
19. Tseng TC, Kuo SW (2018) Hierarchical self-assembled structures from Diblock copolymer mixtures by competitive hydrogen bonding strength. Molecules 23:2242
20. Tseng TC, Kuo SW (2018) Hydrogen-bonding strength influences hierarchical self-assembled structures in unusual miscible/immiscible Diblock copolymer blends. Macromolecules 51:6451–6459
21. Soler-IIIia GJ, Crepaldi EL, Grosso D, Sanchez C (2003) Block copolymer-templated mesoporous oxides. Curr Opin Colloid Interface Sci 8:109–126
22. Wei J, Wang H, Deng Y, Sun Z, Shi L, Tu B, Luqman M, Zhao D (2011) Solvent evaporation induced aggregating assembly approach to three-dimensional ordered mesoporous silica with ultralarge accessible mesopores. J Am Chem Soc 133:20369–20377
23. Li JG, Chen WC, Kuo SW (2012) Phase behavior of mesoporous silicas templated by the amphiphilic diblock copolymer poly (ethylene-b-ethylene oxide). Microporous Mesoporous Mater 163:34–41
24. Altukhov O, Kuo SW (2015) Crystallization ability of poly (lactic acid) block segments in templating poly(ethylene oxide-b-lactic acid) diblock copolymers affects the resulting structures of mesoporous silicas. RSC Adv 5:22625–22637
25. Liu CC, Chu WC, Li JG, Kuo SW (2014) Mediated competitive hydrogen bonding form mesoporous phenolic resins templated by poly(ethylene oxide-b-ε-caprolactone-b-l-lactide) triblock copolymers. Macromolecules 47:6389–6400
26. Zhao D, Feng J, Huo Q, Melosh N, Fredrickson GH, Chmelka BF, Stucky GD (1998) Triblock copolymer syntheses of mesoporous silica with periodic 50 to 300 angstrom pores. Science 279:548–552
27. Chu WC, Chiang SF, Li JG, Kuo SW (2014) Mesoporous silicas templated by symmetrical multiblock copolymers through evaporation-induced self-assembly. RSC Adv 4:784–793
28. Kosonen H, Ruokolainen J, Torkkeli M, Serimaa R, Nyholm P, Ikkala O (2002) Micro- and macrophase separation in phenolic resol resin/PEO-PPO-PEO block copolymer blends: effect of hydrogen-bonded PEO length. Macromol Chem Phys 203:388–392
29. Liang C, Dai S (2006) Synthesis of mesoporous carbon materials via enhanced hydrogen-bonding interaction. J Am Chem Soc 128: 5316–5317
30. Meng Y, Gu D, Zhang F, Shi Y, Cheng L, Feng D, Wu Z, Chen Z, Wan Y, Stein A, Zhao D (2006) A family of highly ordered mesoporous polymer resin and carbon structures from organic-organic self-assembly. Chem Mater 18:4447–4464
31. Chu WC, Chiang SF, Li JG, Kuo SW (2013) Hydrogen bonding-mediated microphase separation during the formation of mesoporous novolac-type phenolic resin templated by the triblock copolymer, PEO-b-PPO-b-PEO. Materials 6:5077–5093
32. Deng Y, Yu T, Wang Y, Shi Y, Meng Y, Gu D, Zhang L, Huang Y, Liu C, Wu X, Zhao D (2007) Ordered mesoporous silicas and carbons with large accessible pores templated from amphiphilic diblock copolymer poly(ethylene oxide)-b-polystyrene. J Am Chem Soc 29:1690–1697
33. Bloch E, Llewellyn PL, Phan T, Bertin D, Hornebecq V (2009) On defining a simple empirical relationship to predict the pore size of mesoporous silicas prepared from PEO-b-PS diblock copolymers. Chem Mater 21:48–55
34. Hu D, Xu Z, Zeng K, Zheng S (2010) From self-organized Novolac resins to ordered nanoporous carbons. Macromolecules 43:2960–2969
35. Deng Y, Liu C, Gu D, Yu T, Tu B, Zhao D (2008) Thick wall mesoporous carbons with a large pore structure templated from a weakly hydrophobic PEO–PMMA diblock copolymer. J Mater Chem 18:91–97
36. Li JG, Lin YD, Kuo SW (2011) From ficrophase separation to self-organized mesoporous phenolic resin through competitive hydrogen bonding with double-crystalline diblock copolymers of poly(-ethylene oxide-b-ε-caprolactone). Macromolecules 44:9295–9309

37. Li JG, Chung CY, Kuo SW (2012) Transformations and enhanced long-range ordering of mesoporous phenolic resin templated by poly (ethylene oxide-b-ε-caprolactone) block copolymers blended with star poly (ethylene oxide)-functionalized silsesquioxane (POSS). J Mater Chem 22:18583–18595
38. Chu WC, Bastakoti BP, Kaneti YV, Li JG, Alamri HR, Alothman ZA, Yamauchi Y, Kuo SW (2017) Tailored Design of Bicontinuous Gyroid Mesoporous Carbon and Nitrogen-Doped Carbon from poly(ethylene oxide-b-caprolactone) Diblock copolymers. Chem Eur J 23:13734–13741
39. Li JG, Ho YF, Ahmed MMM, Liang HC, Kuo SW (2019) Mesoporous carbons Templated by PEO-PCL block copolymers as electrode materials for Supercapacitors. Chem Eur J 25:10456–10463
40. AFM EL-M, Liu TE, Kuo SW (2020) Direct synthesis of nitrogen-doped Mesoporous carbons from Triazine-functionalized Resol for CO_2 uptake and highly efficient removal of dyes. J Hazard Mater 391:122163
41. Werner JG, Hoheisel TN, Wiesner U (2014) Synthesis and characterization of gyroidal mesoporous carbons and carbon monoliths with tunable ultralarge pore size. ACS Nano 8:731–743
42. Deng Y, Liu J, Liu C, Gu D, Sun Z, Wei J, Zhang J, Tu B, Zhao D (2008) Ultra-large-pore mesoporous carbons templated from poly(-ethylene oxide)-b-polystyrene diblock copolymer by adding polystyrene homopolymer as a pore expander. Chem Mater 20:7281–7286
43. Wei J, Deng Y, Zhang J, Sun Z, Tu B, Zhao D (2011) Large-pore ordered mesoporous carbons with tunable structures and pore sizes. Solid State Sci 13:784–792
44. Kuo SW, Lin CL, Chang FC (2002) Phase behavior and hydrogen bonding in ternary polymer blends of phenolic resin/poly(ethylene oxide)/poly(ε-caprolactone). Macromolecules 35:278–285
45. Kuo SW (2008) Hydrogen-bonding in polymer blends. J Polym Res 15:459–486
46. Hsu JY, Hsieh IF, Nandan B, Chiu FC, Chen JH, Jeng US, Chen HL (2007) Crystallization kinetics and crystallization-induced morphological formation in the blends of poly(ε-caprolactone)-block-polybutadiene and Polybutadiene Homopolymer. Macromolecules 40:5014–5022
47. Ahmed DS, El-Hiti GA, Yousif E, Ali AA, Hameed AS (2018) Design and synthesis of porous polymeric materials and their applications in gas capture and storage: a review. J Polym Res 25:75
48. Zhang J, Qiao ZA, Mahurin SM, Jiang X, Chai SH, Lu H, Nelson K, Dai S (2015) Hypercrosslinked phenolic polymers with well-developed Mesoporous frameworks. Angew Chem Int Ed 54:4582–4586
49. Li G, Zhang B, Yan J, Wang Z (2014) Tetraphenyladamantane-based Polyaminals for highly efficient captures of CO2 and organic vapors. Macromolecules 47:6664–6670
50. Yu L, Hu L, Anasori B, Liu YT, Zhu Q, Zhang P, Gogotsi Y, Xu B (2018) MXene-bonded activated carbon as a flexible electrode for high-performance Supercapacitors. ACS Energy Lett 3:1597–1603
51. Farzana R, Rajarao R, Bhat BR, Sahajwalla V (2018) Performance of an activated carbon Supercapacitor electrode synthesised from waste compact discs (CDs). J Ind Eng Chem 65:387–396
52. Abioye AM, Ani FN (2015) Recent development in the production of activated carbon electrodes from agricultural waste biomass for Supercapacitors: a review. Renew Sust Energ Rev 52:1282–1293
53. Wang D, Fang G, Xue T, Ma J, Geng GA (2016) Melt route for the synthesis of activated carbon derived from carton box for high performance symmetric Supercapacitor applications. J. Power Sources 307:401–409
54. Zhou X, Chen Q, Wang A, Xu J, Wu S, Shen J (2016) Bamboo-like composites of V_2O_5 /Polyindole and activated carbon cloth as electrodes for all-solid-state flexible asymmetric Supercapacitors. ACS Appl Mater Interfaces 8:3776–3783

Publisher's note Springer Nature remains neutral with regard to jurisdictional claims in published maps and institutional affiliations.